

# Machine learning molecular dynamics insight into high interface stability and fast kinetics of low-cost magnesium chloride amine electrolyte for rechargeable magnesium batteries

Haiming Hua<sup>1</sup>, Fei Wang<sup>1</sup>, Feng Wang, Jiayue Wu, Yaoqi Xu, Yichao Zhuang, Jing Zeng<sup>\*</sup>, Jinbao Zhao<sup>\*</sup>

College of Chemistry and Chemical Engineering, Xiamen University, Xiamen 361005, PR China, State-Province Joint Engineering Laboratory of Power Source Technology for New Energy Vehicle, State Key Laboratory of Physical Chemistry of Solid Surfaces, Engineering Research Center of Electrochemical Technology, Ministry of Education, Collaborative Innovation Center of Chemistry for Energy Materials, Xiamen University, Xiamen, 361005, PR China

## ARTICLE INFO

### Keywords:

Machine learning molecular dynamics  
Accurate solvation structure  
High interface stability  
Fast kinetics  
Rechargeable magnesium batteries

## ABSTRACT

The development of rechargeable magnesium batteries (RMBs) is hindered by the lack of long-lifespan and low-cost electrolytes. Moreover, due to lacking of an in-depth understanding of accurate dynamic solvation structures, the relationship between the interface kinetics behavior and a stable anode interface is still unclear. Herein, we develop a novel low-cost electrolyte containing the MgCl<sub>2</sub> salt and the 3-methoxypropylamine solvent (denoted as the MgCl<sub>2</sub>-S2 electrolyte), which exhibits higher interface stability and faster kinetics compared to the reference Mg(TFSI)<sub>2</sub>-S2 electrolyte. The powerful machine learning molecular dynamics (MLMD) is employed to systematically investigate the differences of the fine solvation structures and explore the fundamental reason for better interfacial dynamics processes. The results show that the degree of dissociation in MgCl<sub>2</sub>-S2 electrolyte is less than 1 %, much lower than 95.1 % in Mg(TFSI)<sub>2</sub>-S2 electrolyte. The solvation structures dominated by Cl<sup>-</sup> ions can induce Mg<sup>2+</sup> ions to preferentially acquire electrons in both kinetics and thermodynamics, which thus improving the deposition kinetics and enhancing the stability of the anode interface. This work inspires a new paradigm from MLMD to investigate the relationship between interface stability and accurate solvation structures for RMBs.

## 1. Introduction

The great advancement of technologies such as smart devices, electric transportation, and large-scale energy storage stations has generated a growing demand for secondary batteries with higher energy density, better safety, and lower raw material costs. Conventional lithium-ion batteries (LIBs) encounter mounting challenges in light of safety concerns and a shortage of Li resources [1-3]. In contrast, rechargeable magnesium batteries (RMBs) have attracted great attention in recent years because RMBs possess outstanding advantages of high safety and low cost attributed to the application of Mg metal anode [4-12]. Furthermore, the Mg metal is capable of transferring two electrons during charge and discharge processes, placing it at the forefront in terms of the energy density among various metal batteries [13-16]. However, due to the multivalent nature of Mg metal, its charge transfer

kinetics is sluggish and the naturally formed solid-electrolyte interphase (SEI) can not readily facilitate the conduction of Mg<sup>2+</sup> ions, resulting in a large polarization and irreversible Mg plating/stripping during cycling [17,18]. Consequently, establishing a stable interface for rapid Mg plating/stripping process remains a formidable challenge.

The common solutions are to develop reductively stable electrolytes [19-30] to avoid the decomposition of electrolyte components and the formation of passivation layers or construct the artificial SEI to form Mg<sup>2+</sup> conducting channels [31-42], but these strategies still face intractable problems to meet the criteria for commercialization, such as high cost, complex preparation process and strict experimental repetition conditions. Therefore, based on the current state of research about Mg metal anode, modification of conventional electrolytes (commercial Mg salts dissolved in commercial solvents) to realize reversible Mg plating/stripping is one of the most promising ways to commercialize

\* Corresponding authors.

E-mail addresses: [zengjing@xmu.edu.cn](mailto:zengjing@xmu.edu.cn) (J. Zeng), [jbzhaob@xmu.edu.cn](mailto:jbzhaob@xmu.edu.cn) (J. Zhao).

<sup>1</sup> H.H. and F.W. contributed equally to this work.

RMBs at present. To solve the problem of anode passivation in the conventional electrolytes, many research groups have demonstrated the feasibility of improving the reversibility of the Mg metal anode by regulating the solvation structures of  $\text{Mg}^{2+}$  ions in electrolytes [43-48]. For example, Wang et al. introduced a series of methoxyethyl-amine additives to optimize the solvation structure of  $\text{Mg}^{2+}$  ions in the 1, 2-dimethoxyethane (DME)-based electrolyte. This solvation sheath reorganization benefits to not only promote interfacial kinetics but also suppress decomposition of the DME molecules [49]. Besides, our previous work elaborately regulated the  $\text{Mg}^{2+}$  solvated structures by designing a series of solvent molecules and proposed a two-step Mg deposition model, including the charge transfer process and the desolvation process, which revealed the important relationship between solvation structures and electrochemical performances in RMBs [50]. However, although the optimization design of solvents can effectively improve the charge transfer kinetics and achieve the reversible Mg plating/stripping behaviors, the issue of facile decomposition of anions in the electrolyte still exists, leading to the failure of the stable interface and limiting the cycle life of the Mg metal anode. And thus, a highly stable interface requires that the anions in the electrolyte should avoid continuous and uncontrollable decomposition to ensure the high cycle stability of the Mg metal anode.

Moreover, in order to design an electrolyte with fast charge transfer kinetics and high interface stability in plating/stripping process during cycling, in addition to choosing the appropriate solvents and anions, it is also very important to obtain accurate solvation structure and establish its relationship with ion deposition kinetics and decomposition mechanism. However, obtaining precise ion solvation structures is currently a challenge in both experiments and computational simulations. In liquid systems, the rapid thermal movement of microstructures makes it difficult to observe structural changes comprehensively by spectroscopic techniques such as vibrational spectroscopy, nuclear magnetic resonance (NMR), and X-ray methods. Computational simulations face similar challenges, as achieving a method with both high accuracy and high speed is a difficult task. In details, traditional short-time ab initio molecular dynamics (AIMD) methods lack of enough time scale, while classical molecular dynamics (CMD) methods lack of accuracy of atomic force. This challenge is particularly pronounced when dealing with  $\text{Mg}^{2+}$  ions, as the high charge density brings by bivalence and the use of asymmetric chelating solvents result in a more complex chemical space in the coordination structure. Fortunately, machine learning molecular dynamics (MLMD) offers a promising solution by significantly improving the calculation speed of energy and force at the ab initio accuracy by several orders of magnitude in molecular dynamics simulations. MLMD has been successfully practiced in the field of electrolytes for LIBs and has provided an in-depth explanation of the conformational relationships of redox reactions based on precise and dynamic solvation structures, which cannot be obtained by CMD or AIMD. Thus, it also hopefully enabling the accurate simulation of Mg electrolyte despite its complexity. [51-54]

In this work, we develop a novel low-cost electrolyte containing a simple  $\text{MgCl}_2$  salt and the optimized 3-methoxypropylamine (denoted as S2) solvent. Electrochemical test results suggests that the  $\text{MgCl}_2$ -S2 electrolyte exhibits an ultra-long cycle life in Mg//stainless steel (SS) asymmetric cell for over 4500 cycles (about 12 months) with an outstanding Coulombic efficiency (CE) about 99.2 %, indicating the  $\text{MgCl}_2$ -S2 electrolyte possesses a more stable interface and faster charge transfer kinetics than those of the reference  $\text{Mg}(\text{TFSI})_2$ -S2 electrolyte. MLMD is employed to gain insight into both the  $\text{MgCl}_2$ -S2 and the reference  $\text{Mg}(\text{TFSI})_2$ -S2 electrolytes, aiming to understand the differences of solvation structures and dynamics of interface processes in these two systems combined with the experimental results. Accurate solvation structures, along with their proportions and the rate of mutual transformation are obtained. Furthermore, the electronic structures based on these accurate dynamic structures are comprehensively studied. These analyses are essential for studying interface but proved

challenging to obtain by using traditional methods. The calculational and experimental results indicate that anions in the  $\text{MgCl}_2$ -S2 electrolyte can more easily enter the  $\text{Mg}^{2+}$  solvation layer than the  $\text{Mg}(\text{TFSI})_2$ -S2 electrolyte, which changes the energy band structure of the electrolyte so that  $\text{Mg}^{2+}$  ions can gain electrons in preference to anions in thermodynamics, thus enhancing the stability of the interface. Moreover,  $\text{Cl}^-$  ions in solvated sheath partially shield the high charge density of  $\text{Mg}^{2+}$  ions, thereby improving the desolvation rate by nearly 3 times, and further improving the deposition kinetics. This work exhibits an in-depth investigation of accurate solvation structure of  $\text{Mg}^{2+}$  ions via the MLMD method, inspiring a new paradigm from MLMD to study interface reaction and develop the high-effectively electrolytes.

## 2. Results and discussion

The classical  $\text{MgCl}_2$  salt, as a simple Mg salt due to the monatomic nature of its anion, is usually employed as the co-salt or additive in electrolytes to improve the passivation of Mg metal anode. Although the price of the  $\text{MgCl}_2$  salt is much lower than that of the common  $\text{Mg}(\text{TFSI})_2$  salt (~5 \$/kg for the  $\text{MgCl}_2$  salt while ~3700 \$/kg for the  $\text{Mg}(\text{TFSI})_2$  salt), it is rarely used as the only solute in the electrolyte of RMBs. The main reason is that the poor solubility of the  $\text{MgCl}_2$  salt in traditional ether solvents results in an extremely low conductivity and concentration of  $\text{Mg}^{2+}$  ions, which cannot support fast anion and cation transport at the normal current density. Interestingly, the  $\text{MgCl}_2$  salt exhibits a high solubility in the S2 solvent, which is exactly different from the traditional ether solvents. Therefore, we systematically compare the differences in solubilities and electrochemical properties of the  $\text{MgCl}_2$  salt in the S2 solvent and two traditional ether solvents, namely, DME and tetrahydrofuran (THF).

The solubilities and maximum conductivities of three electrolytes are shown in Fig. 1a. For the DME and THF solvents, the solubilities of  $\text{MgCl}_2$  salt are about 0.01 mol/L (M) and 0.25 M with the max conductivities of only 2  $\mu\text{S}/\text{cm}$  and 15  $\mu\text{S}/\text{cm}$ , respectively. However, the solubility of  $\text{MgCl}_2$  in S2 solvent can reach to 1.35 M, which is greatly increased compared with traditional ethers. According to the relationship between conductivity and concentration (Figure S1), the highest conductivity of  $\text{MgCl}_2$  salt in S2 solvent is 153.8  $\mu\text{S}/\text{cm}$  at 0.5 M. The electrochemical performances about Mg plating/stripping behaviors of three electrolytes are acquired by cyclic voltammetry (CV) measurement with a three-electrode test system (Fig. 1b). The redox peaks of the  $\text{MgCl}_2$ -S2 electrolyte are much higher than those of THF and DME solvents, indicating the fast kinetics and highly reversible Mg plating/stripping behavior can be obtained by the  $\text{MgCl}_2$ -S2 electrolyte, which is attributed to the sufficient anion-cation pairs to support fast electromigration in the electrolyte and high compatibility of the S2 solvent to the Mg metal anode.

In order to further investigate the reason for the different solubilities for  $\text{MgCl}_2$  salt in three solvents, the interaction between solvents and the  $\text{MgCl}_2$  salt are further studied by AIMD and density functional theory (DFT) calculation. The dissolution energy change ( $E_{\text{sol}}$ ) obtained by AIMD and the binding energy ( $E_{\text{b}}$ ) obtained by DFT are shown in Fig. 1c, and the electrostatic potential (ESP) surface penetration diagram of the solvent binding with each ion are shown in Fig. 1d. The  $E_{\text{sol}}$  of the  $\text{MgCl}_2$  salt in S2, THF and DME solvents are -194.8, -74.7 and -61.0 kJ/mol, respectively, which is consistent with the trend of their solubilities. The identical trend indicates that the increase in solubility is due to the enhancement of solute-solvent interaction. The  $E_{\text{b}}$  of S2 with  $\text{Mg}^{2+}$  ion and  $\text{Cl}^-$  ion are -170.3 and -15.8 kJ/mol, respectively, much more negative than those of THF (-118.9 and -6.5 kJ/mol, respectively) and DME (-93.5 and -2.5 kJ/mol, respectively), indicating that the S2 solvent is more likely to combine with both  $\text{Mg}^{2+}$  and  $\text{Cl}^-$  ions (Fig. 1c). Obviously, the increase in solute-solvent interaction is mainly due to the introduction of  $-\text{NH}_2$ . The ESP values near N and H atoms of amino groups are -183.8 and 112.6 kJ/mol, respectively (Fig. 1a). The more favorable negative and positive ESP values in S2 than in THF and DME

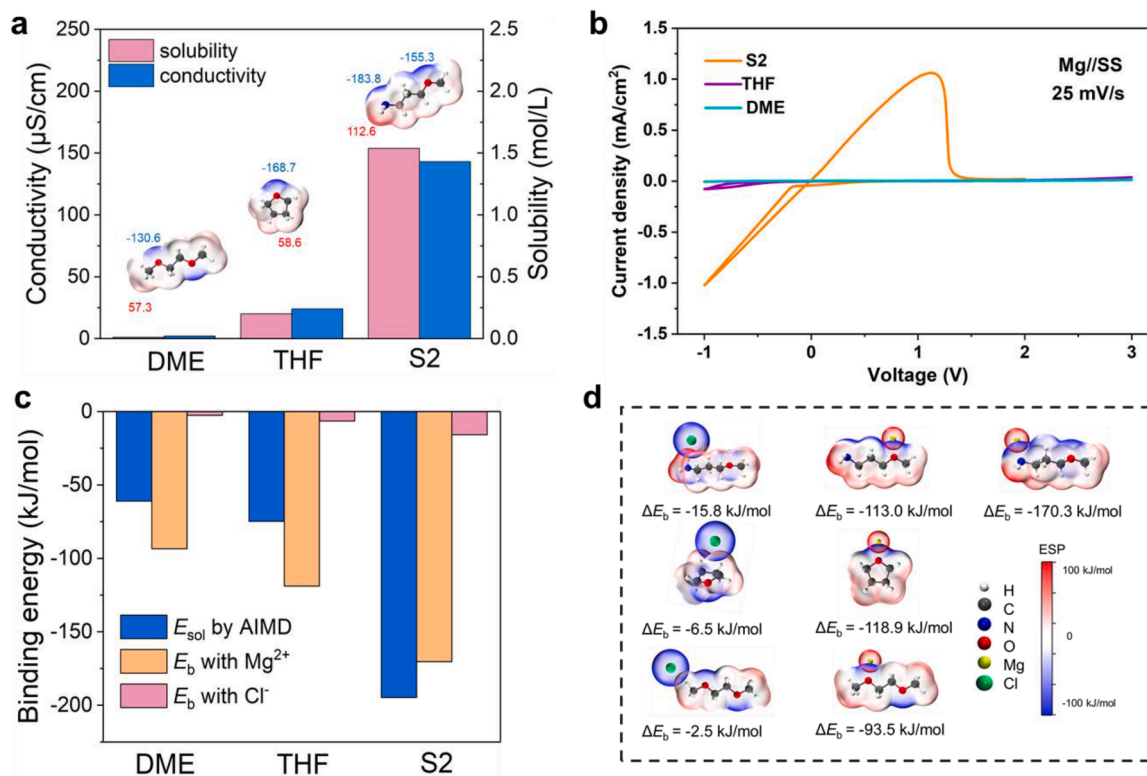


**Fig. 1.** a) The solubilities and max conductivities of  $\text{MgCl}_2$  in S2, THF and DME solvents. ESP diagrams of solvents are inserted above the bar charts. The extremes of ESP values are marked in kcal/mol. b) The CV curves of  $\text{MgCl}_2$  salt in S2, THF and DME solvents at the scan rate of 25 mV/s. c) The  $E_{\text{sol}}$  of  $\text{MgCl}_2$  in different solvents by AIMD and  $E_{\text{b}}$  of solvents with  $\text{Cl}^-$  ion or  $\text{Mg}^{2+}$  ion. d) ESP surface penetration diagrams of the solvents binding with each ion.

indicate that amino groups carry more negative and positive charges to stabilize the  $\text{MgCl}_2$  salt and form the stable electrolyte (Fig. 1a).

The Mg plating/stripping behaviors of  $\text{MgCl}_2$ -S2 electrolytes with different  $\text{MgCl}_2$  concentrations are investigated by CV measurements. As shown in Fig. 2a, the 0.5 M  $\text{MgCl}_2$ -S2 electrolyte shows the highest redox peaks, which is in the agreement with the conductivity test results. The electrolyte with a higher concentration of  $\text{MgCl}_2$ , such as 0.7 M, exhibits a lower response current, which is mainly caused by the limitation of the electrolyte viscosity. As expected, the 0.5 M  $\text{MgCl}_2$ -S2 electrolyte can stably support a Mg plating/stripping cycle during CV test (Fig. 2b). The linear-sweep voltammetry (LSV) results of the 0.5 M  $\text{MgCl}_2$ -S2 electrolyte are also shown in Figure S2. The CE as a significant criterion for the reversibility of the Mg metal anode is also investigated (Fig. 2c). The Mg//SS asymmetric cell with the 0.5 M  $\text{MgCl}_2$ -S2 electrolyte can run stably for 4500 cycles (about 12 months) with an outstanding average CE of over 99.2 %, confirming the excellent interface stability of Mg metal with the simple  $\text{MgCl}_2$  salt and the optimized S2 electrolyte system. To the best of our knowledge, compared with other novel amine electrolytes developed in recent years, such a long cycle life and average CE is the superior among these literatures so far (Fig. 2d). Additionally, attributed to the strong hydrogen bond interaction between amine groups and water molecules, the electrochemical performance of 0.5 M  $\text{MgCl}_2$ -S2 electrolyte can be well maintained even with the addition of 10,000 ppm  $\text{H}_2\text{O}$  into the electrolyte. As shown in Fig. 2e, the Mg//SS cell shows a reversible Mg plating/stripping behavior after several activation process and exhibits a satisfied CE of about 95 %, indicating the good water-resistant property of the  $\text{MgCl}_2$ -S2 electrolyte. This outstanding water resistance of the novel electrolyte enable ordinary purity reagents can be used to produce electrolytes directly instead of expensive ultra-dry reagents, which further reduces the raw materials cost of batteries. In addition, the compatibility of the 0.5 M  $\text{MgCl}_2$ -S2 electrolyte with the cathode is verified by the classical  $\text{Mo}_6\text{S}_8$  materials as well (Figure S3a-b).

The electrochemical properties of the electrolyte are deeply influenced by the solvation structures of anions and cations in electrolytes. Therefore, insight into the solvation structure of the  $\text{MgCl}_2$ -S2 electrolyte is essential for deeply finding out the structure-activity relationship between the solvation structure and interface stability. The molecular dynamics simulation method is one of the most powerful methods to study the microstructure of electrolyte. However, due to the coordination competition between various coordination atoms, O atoms, Cl atoms and N atoms with  $\text{Mg}^{2+}$  ions in the system, the real solvation structures are difficult to be described accurately by AIMD or CMD, which represents the two most commonly used MD methods at present. The AIMD lacks sufficient statistical sampling due to the huge amount of calculation, while the classical MD lacks the accuracy of inter-atomic energy and force due to the empirical parameters. And thus, we choose the Deep potential molecular dynamics [55] (DeepPMD) method based on machine learning to in-depth study this complex system. The strategy of concurrent learning is used to fully sample the potential energy surface of electrolytes automatically by DP-GEN [56] and DeepPMD-kit [57] software packages, and DFT calculations are used to compute the corresponding atomic forces and energies. After some iterations of concurrent learning, the machine learning potential (MLP) model can reach convergence and shows ab initio accuracy. Therefore, an MLP model with both ab initio accuracy and classical force field efficiency are obtained. Using MLMD to sample the electrolytes in the order of tens of nanoseconds, the ion solvation structures and the rates of ligand exchange in the electrolytes can be accurately captured. MLP models for  $\text{MgCl}_2$  electrolytes and  $\text{Mg}(\text{TFSI})_2$  electrolytes are trained in this work, as the latter serves as the reference because the  $\text{MgCl}_2$  and  $\text{Mg}(\text{TFSI})_2$  are two classical and widely used salts in RMBs which thus is greatly deserved to in-depth investigated.

The process of training MLP is shown in Fig. 3a. First, CMD and AIMD are used to construct some initial structures of the  $\text{MgCl}_2$ -S2 electrolytes and the  $\text{Mg}(\text{TFSI})_2$ -S2 electrolytes at different concentrations to ensure

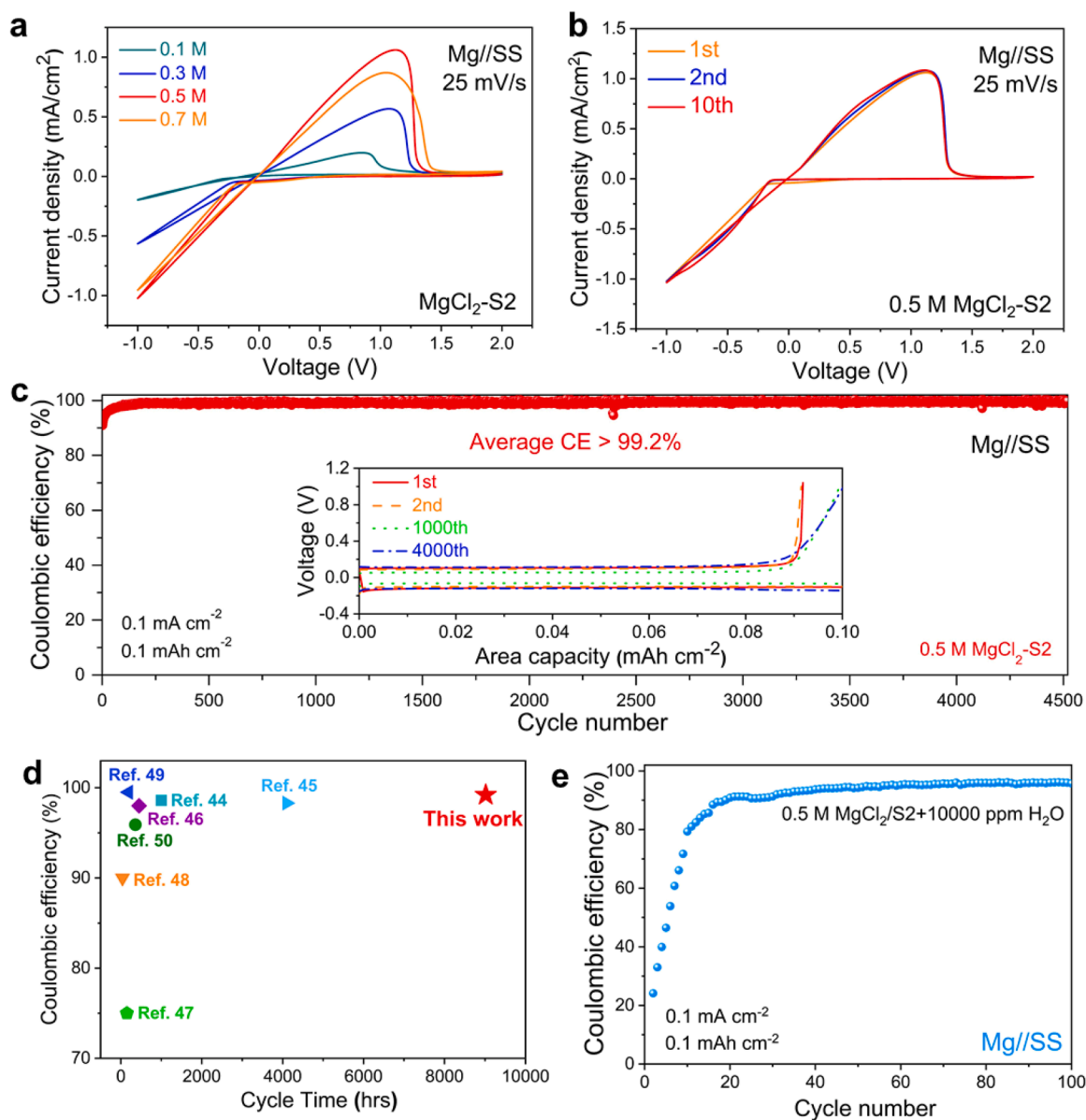


**Fig. 2.** a) The CV curves of MgCl<sub>2</sub> salt in the S2 solvent at different concentrations. b) The first, second and tenth cycles CV curves of the 0.5 M MgCl<sub>2</sub>-S2 electrolyte. c) The CE of Mg//SS asymmetric cell at 0.1 mA cm<sup>-2</sup> for 0.1 mAh cm<sup>-2</sup> (Insert is the corresponding voltage profiles of the Mg//SS asymmetric cell). d) Comparison of cycling time and average CE in this work with reported data in literatures. e) The CE of Mg//SS asymmetric cell of the 0.5 M MgCl<sub>2</sub>-S2 electrolyte with the addition of 10,000 ppm H<sub>2</sub>O.

the model is fully sampled. MLP training is carried out by iterative way, and the process is divided into labeling, training and exploration. In the labeling step, the energies and atomic forces of the initial structures or candidate structures selected from the previous iteration are calculated by the DFT method; In the training step, the neural network model is used to construct the mapping from the atomic local structures to atomic forces and energies, and four MLP models are trained with different neural network parameters. In the exploration step, the MLMD is performed by using the above four MLP models. The accuracy of the models is evaluated by the maximum root mean square errors (RMSEs) of atomic forces over four MLP models. Some candidate structures with medium error are randomly selected for the next iteration. In each iteration, if the number of candidate structures ( $N_{\text{new}}$ ) is greater than the threshold, then enter the next iteration; otherwise, exit the loop. When  $N_{\text{new}}$  is less than the threshold after several iterations, the iteration reaches convergence. And thus, the MLP which can well describe the potential energy surface of the electrolytes is obtained. After the MLP

models of MgCl<sub>2</sub> and Mg(TFSI)<sub>2</sub> electrolytes are both trained and converged, respectively, the accuracy of MLP models are tested. In the **Figure S4a,b**, there is a fairly good linear correlation between the MLP model and the DFT. The RMSE of models for MgCl<sub>2</sub> and Mg(TFSI)<sub>2</sub> electrolytes are only  $6.3 \times 10^{-2}$  and  $6.8 \times 10^{-2}$  eV/Å, respectively, which indicates that the trained MLP models have the DFT-level accuracy. Simulation boxes containing over 3000 atoms for the two electrolytes are built to ensure sufficient spatial scale, and the annealing method combined with the simulation time of more than 40 ns is performed to ensure sufficient time scale. The MD simulation snapshot and corresponding radial distribution function (RDF) diagram are shown in the **Fig. 3b**. In the MgCl<sub>2</sub>-S2 electrolyte, the coordination numbers of N, O and Cl atoms to Mg<sup>2+</sup> ions are 3.65, 0.63 and 1.52, respectively, and the total coordination number is 5.80. In the Mg(TFSI)<sub>2</sub>-S2 electrolyte, the coordination numbers of N, O atoms of the S2 solvent and O of TFSI<sup>-</sup> anions to Mg<sup>2+</sup> ions are 3.97, 1.82 and 0.04, respectively, and the total coordination number is 5.83. The difference of coordination numbers

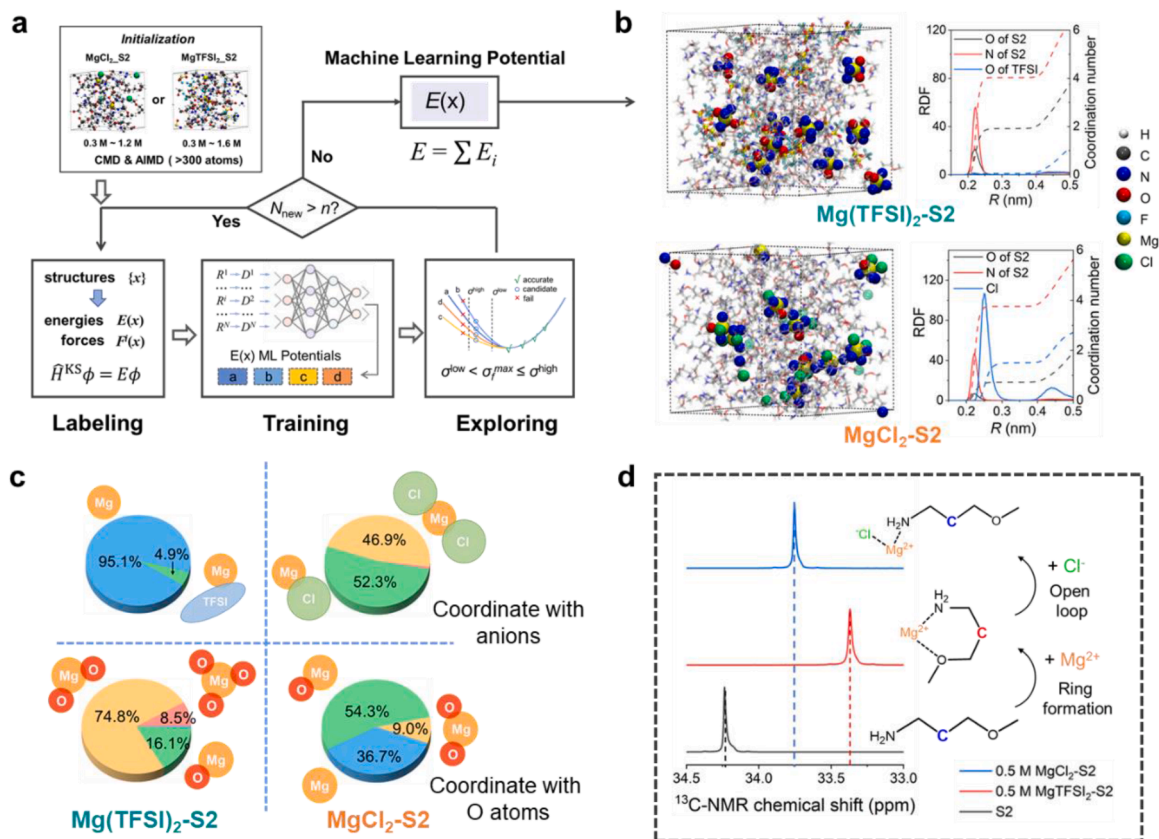


Fig. 3. a) Schematic illustration of ML potential training process. b) Snapshots and RDF of MLMD trajectories of the  $\text{Mg}(\text{TFSI})_2\text{-S2}$  and  $\text{MgCl}_2\text{-S2}$  electrolytes. c) Distribution of solvated ions in MLMD trajectories. d)  $^{13}\text{C}$ -NMR spectra of  $\beta\text{-C}$  of S2 in pure S2, 0.5 M  $\text{Mg}(\text{TFSI})_2\text{-S2}$  and 0.5 M  $\text{MgCl}_2\text{-S2}$  electrolytes.

indicates that the electrolytes formed in the  $\text{MgCl}_2\text{-S2}$  electrolyte and  $\text{Mg}(\text{TFSI})_2\text{-S2}$  electrolyte has completely different solvation structures. According to the RDF results, the association of anions and cations in the  $\text{Mg}(\text{TFSI})_2$  electrolyte is very slight, while in the  $\text{MgCl}_2\text{-S2}$  electrolyte, most  $\text{Mg}^{2+}$  ions are combined with  $\text{Cl}^-$  ions. Besides, as for the S2 solvent, the N atom has a stronger coordination trend with  $\text{Mg}^{2+}$  ion than the O atom, which is consistent with the ESP of S2 molecule (Fig. 1a). We then perform a more detailed analysis of the simulated trajectory to obtain more information about the coordination structures. As shown in the Fig. 3c, in the  $\text{Mg}(\text{TFSI})_2\text{-S2}$  electrolyte, anions and cations are almost dissociated, as the degree of dissociation is 95.1%. And in the  $\text{MgCl}_2\text{-S2}$  electrolyte, 52.3% of  $\text{Mg}^{2+}$  ion is associated with one  $\text{Cl}^-$  ion, while 46.9% of  $\text{Mg}^{2+}$  ion is associated with two  $\text{Cl}^-$  ions, and almost no unassociated  $\text{Mg}^{2+}$  ions exist. The almost complete dissociation in the  $\text{Mg}(\text{TFSI})_2\text{-S2}$  electrolyte is due to the dispersion of negative charge caused by the large conjugated structure of  $\text{TFSI}^-$ . While the negative charge of  $\text{Cl}^-$  in the  $\text{MgCl}_2\text{-S2}$  electrolyte is concentrated, resulting in a strong binding ability with the cation. The difference in the degree of association degree also explains the difference of the conductivities of the  $\text{MgCl}_2\text{-S2}$  electrolyte and the  $\text{Mg}(\text{TFSI})_2\text{-S2}$  electrolyte at the same concentration.

In order to investigate the participation of S2 molecules in the first solvation layer of  $\text{Mg}^{2+}$  ions, the combination situation of  $\text{Mg}^{2+}$  ions with O atoms is also counted. In the  $\text{Mg}(\text{TFSI})_2\text{-S2}$  electrolyte,  $\text{Mg}^{2+}$  ions coordinated with three, two or one O atoms account for 8.5%, 74.8% and 16.1%, respectively. In the  $\text{MgCl}_2\text{-S2}$  electrolyte, almost no Mg ions coordinate with three oxygen atoms, and the  $\text{Mg}^{2+}$  ions coordinated with two, one or zero O atoms account for 9.0%, 54.3% and 36.7%, respectively. It can be seen that after  $\text{Cl}^-$  ions enter the first solvation layer of  $\text{Mg}^{2+}$  ions and a part of O atoms is squeezed out. Combined with the RDF data (Fig. 3b), the coordination number of the N atom in the S2 solvent decreases by 0.32, while the coordination number of the O atom

in the S2 decreases by 1.19. Therefore,  $\text{Cl}^-$  ions mainly replace the coordination sites of O atoms, and secondly replace the coordination sites of N atoms, which is consistent with the order of the ESP of N and O atoms (Fig. 1a). The  $^{13}\text{C}$  NMR spectroscopy further verifies the change of the coordination structure (Fig. 3d). The chemical shift of  $\beta\text{-C}$  of S2 in the pure S2 solvent, the  $\text{Mg}(\text{TFSI})_2\text{-S2}$  electrolyte and the  $\text{MgCl}_2\text{-S2}$  electrolyte are 34.25 ppm, 33.34 ppm and 33.7 ppm, respectively. The obvious shift compared the pure S2 solvent with the  $\text{Mg}(\text{TFSI})_2\text{-S2}$  electrolyte is possibly caused by the comprehensive result of ring tension and electronic effect [58-60]. The pure S2 solvents mainly present an extended conformation, and after adding  $\text{Mg}^{2+}$  ions, part of S2 solvents chelate with  $\text{Mg}^{2+}$  ions and show ring shape structures, causing the chemical shift to move to a higher field. When the  $\text{Cl}^-$  ions enter the first solvation layers of  $\text{Mg}^{2+}$  ions, because part of the oxygen atoms is extruded from the first solvated structures, some S2 solvents resume to stretched again and the chemical shift of  $\beta\text{-C}$  returns to the low field partially. The  $^{13}\text{C}$  NMR spectroscopy of electrolytes with more concentrations are shown in Figure S5. The same trend of chemical shift change further confirms the change in coordination configuration of the S2 solvent. The precise dynamic structures of the electrolytes obtained through MLMD will be used to investigate the reduction stability of electrolytes and ion deposition kinetics of  $\text{Mg}^{2+}$  ions in later chapters.

The interface stability of the Mg metal anode for the  $\text{MgCl}_2\text{-S2}$  electrolyte and the  $\text{Mg}(\text{TFSI})_2\text{-S2}$  electrolyte is further investigated in Mg//Mg symmetric cells (Fig. 4a). Although the  $\text{Mg}(\text{TFSI})_2\text{-S2}$  electrolyte has a lower overpotential at first several cycles due to its high conductivity compared to the  $\text{MgCl}_2\text{-S2}$  electrolyte, the overpotential continues to increase during cycling and rises sharply after about 2000 h, demonstrating that uncontrollable side reactions lead to the interface state deteriorate continuously. This is also confirmed in the CE test of Mg//SS asymmetric cell for the  $\text{Mg}(\text{TFSI})_2\text{-S2}$  electrolyte (Figure S6a, b). The CE for the  $\text{Mg}(\text{TFSI})_2\text{-S2}$  electrolyte is only 97.8% with a cycle

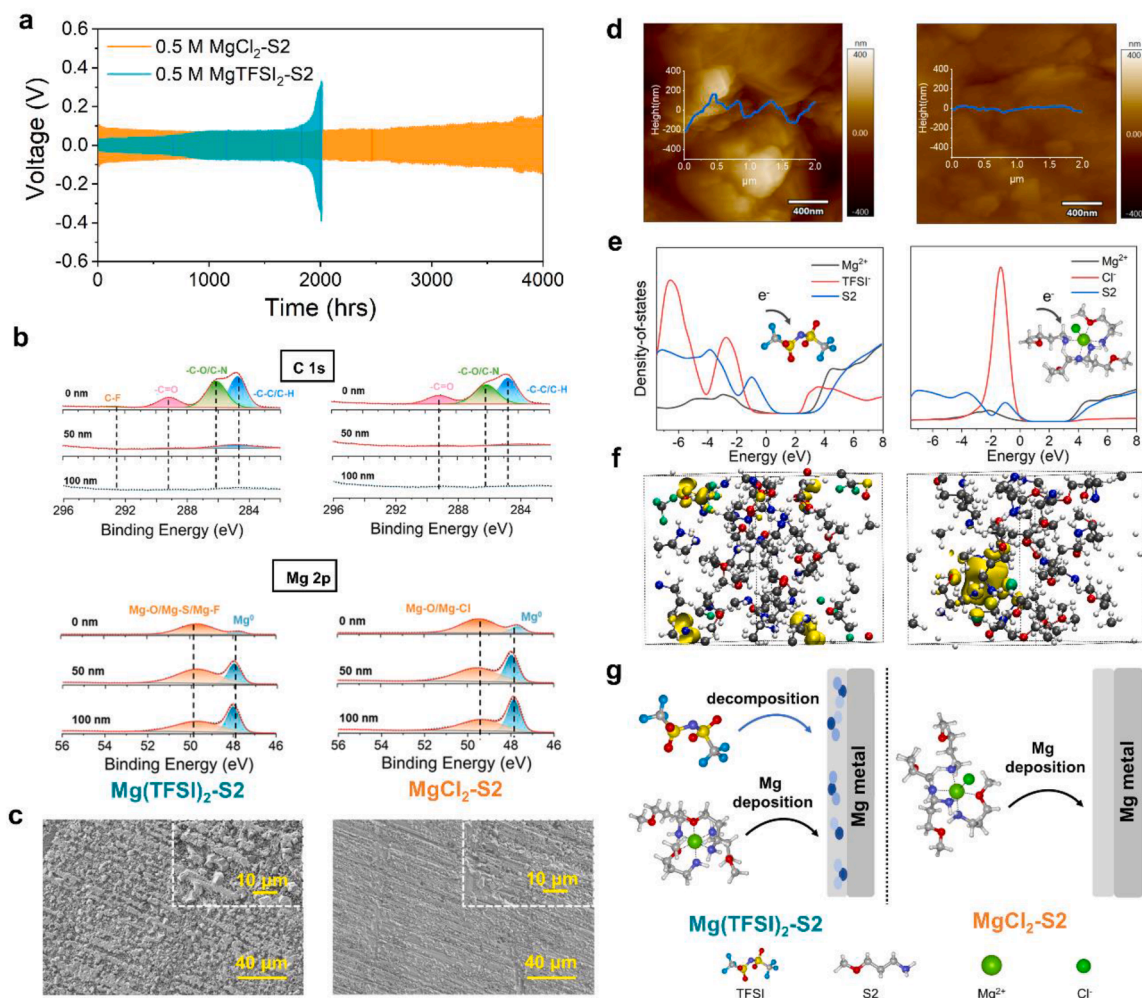


**Fig. 4.** a) Galvanostatic cycling performances of the 0.5 M  $\text{MgCl}_2\text{-S2}$  electrolyte and the 0.5 M  $\text{Mg}(\text{TFSI})_2\text{-S2}$  electrolyte in  $\text{Mg}/\text{Mg}$  symmetric cells at  $0.1 \text{ mA cm}^{-2}$  for  $0.1 \text{ mAh cm}^{-2}$ . b) High-resolution XPS spectra of C 1s and Mg 2p for the 0.5 M  $\text{MgCl}_2\text{-S2}$  electrolyte and the 0.5 M  $\text{Mg}(\text{TFSI})_2\text{-S2}$  electrolyte (cycled at  $0.1 \text{ mA cm}^{-2}$  to  $0.1 \text{ mAh cm}^{-2}$  for 30 cycles). c) SEM images and d) AFM images (inset is the height profiles) of the Mg deposits in the 0.5 M  $\text{Mg}(\text{TFSI})_2\text{-S2}$  (left) or 0.5 M  $\text{MgCl}_2\text{-S2}$  (right) at  $0.1 \text{ mA cm}^{-2}$  with  $0.1 \text{ mAh cm}^{-2}$  for 30 cycles. e) The PDOS diagram of  $\text{MgCl}_2\text{-S2}$  electrolyte and  $\text{Mg}(\text{TFSI})_2\text{-S2}$  electrolyte from MLMD trajectory. f) The Density distribution of inserted excess electron after 50 fs AIMD simulation. Yellow surface is the spin density of excess electron. g) Schematic diagrams depicting the interfacial deposition of Mg anode in  $\text{MgCl}_2\text{-S2}$  electrolyte and  $\text{Mg}(\text{TFSI})_2\text{-S2}$  electrolyte.

life of just 400 cycles, which is obviously below than that of the  $\text{MgCl}_2\text{-S2}$  electrolyte. While for the  $\text{MgCl}_2\text{-S2}$  electrolyte, the overpotential can be stably maintained below 0.15 V and the  $\text{Mg}/\text{Mg}$  symmetric cell can operate stably for over 4000 h, indicating the higher interface stability and the longer cycle life attributed to the optimization design of anions. This explanation is further confirmed by the X-ray photoelectron spectroscopy (XPS) measurement (Fig. 4b) [32,44,45,48,49]. In the C 1s spectrum, the content of C—N and C—C species in the interlayer formed in the  $\text{Mg}(\text{TFSI})_2\text{-S2}$  electrolyte is higher than that in the  $\text{MgCl}_2\text{-S2}$  electrolyte, especially in the depth of 50 nm, which are caused by the decomposition of  $\text{TFSI}^-$  anions. In the Mg 2p spectrum, the content of  $\text{Mg}^0$  in the  $\text{MgCl}_2\text{-S2}$  electrolyte is obviously higher than that in the  $\text{Mg}(\text{TFSI})_2\text{-S2}$  electrolyte at the depths of 0 nm, 50 nm and 100 nm, indicating that the formation of decomposition products in the  $\text{MgCl}_2\text{-S2}$  electrolyte is reduced and the deposition of Mg is promoted. Besides, we conducted an experiment to demonstrate that the electrochemical performance is dominated by the solvation structure rather than the  $\text{Mg}^{2+}$ -conductive interfacial layer (Figure S7). The surface morphology of Mg metal anodes after cycles are observed at different spatial scales by scanning electron microscope (SEM) (Fig. 4c), atomic force microscope (AFM) (Fig. 4d) and laser microscope (Figure S8a,b). It shows that smoother surfaces of Mg deposits nearly without protrusions can be

obtained in the 0.5 M  $\text{MgCl}_2\text{-S2}$  electrolyte compared with the 0.5 M  $\text{Mg}(\text{TFSI})_2\text{-S2}$  electrolyte, indicating the less generation of byproducts and more uniform Mg deposits in the  $\text{MgCl}_2\text{-S2}$  electrolyte.

The electrochemical reactivity of electrolyte is closely related to its electronic structure. In order to study the difference of interface stability between the two electrolytes, projected density of state (PDOS) and excess electron distribution analysis are performed. The average PDOS [61] from nanosecond level of MLMD trajectory reflects the trend of gaining electrons of the system by the valence band partial wave shape in Fig. 4e. In the  $\text{Mg}(\text{TFSI})_2\text{-S2}$  electrolyte, the forefront of the valence band is assigned to  $\text{TFSI}^-$  anion, which indicates that  $\text{TFSI}^-$  anion is easier to obtain electrons than other components in thermodynamics and thus is decomposed to form the passivation layers, although the reduction reaction of  $\text{TFSI}^-$  anion has a much higher Marcus charge transfer energy barrier (67.9 kJ/mol) than solvated  $\text{Mg}^{2+}$  ions (less than 10 kJ/mol) (Table S1), indicating the reduction of  $\text{TFSI}^-$  anion is not easy to occur kinetically. Therefore, decomposition of the  $\text{TFSI}^-$  anion is not apparent in the short term, but can still occur and compete with the reduction of  $\text{Mg}^{2+}$  ions in a long cycle, leading to the degradation of the anode interface. In the  $\text{MgCl}_2\text{-S2}$  electrolyte, the forefront of the valence band is assigned to  $\text{Mg}^{2+}$  ions, indicating that  $\text{Mg}^{2+}$  ions are more susceptible to gain electrons thermodynamically. The density distribution

of inserted excess electron further verifies this trend (Fig. 4f). The inserted excess electrons are mainly distributed on TFSI<sup>-</sup> anions after gaining an electron in the Mg(TFSI)<sub>2</sub>-S2 electrolyte. While for the MgCl<sub>2</sub>-S2 electrolyte, the inserted excess electrons are mainly distributed around Mg<sup>2+</sup> ions after gaining an electron. Thus, a schematic diagram depicting the interfacial deposition can be obtained (Fig. 4g). In the Mg(TFSI)<sub>2</sub>-S2 electrolyte, both anions and solvated Mg<sup>2+</sup> ions can get electrons, resulting in an interface composed of deposited metallic Mg and side reaction products. During a long cycle process, the accumulation of decomposition products leads to the increase of the overpotential gradually, which further aggravates the decomposition of anions and results in the failure of the battery eventually. In sharp contrast, as for the MgCl<sub>2</sub>-S2 electrolyte, attributed to high stability of the Cl<sup>-</sup> anions, a stable interface mostly composed of the Mg deposits can be maintained during the long cycles of plating/stripping process.

The interfacial charge transfer kinetics of the two electrolytes is further investigated. We add the supporting electrolyte 1-butyl-1-methylpyrrolidinium bis(trifluoromethylsulfonyl)imide (PP14TFSI) to regulate conductivities of the two electrolytes close together thus eliminating the interference of solution ohmic impedance. PP14TFSI is selected for its high conductivity, sufficient dissociation and sufficient cation stability. As shown in the Figure S9a,b, the MgCl<sub>2</sub>-S2 electrolyte exhibits the lower charge transfer impedance ( $R_{ct}$ ) and overpotential in the Mg/Mg symmetric cell than that of the Mg(TFSI)<sub>2</sub>-S2 electrolyte, indicating that the MgCl<sub>2</sub>-S2 electrolyte has a faster charge transfer kinetics after controlling the influence of the electromigration of cations and anions in the electrolytes. Although the addition of PP14TFSI has an impact on the dissociation of MgCl<sub>n</sub> species in ether solvents[62], this

effect varies depending on the concentration and type of solvents. The results obtained from the CMD simulation (Figure S10a-d) demonstrate that due to the sufficiently low concentration of MgCl<sub>2</sub> and the sufficiently strong dissociation capacity of the solvent in our electrolytes, PP14TFSI promotes the dissociation of MgCl<sub>n</sub> only to a certain extent without fundamentally altering its structure, thereby enabling a qualitative comparison. The two-step Mg deposition model proposed in our previous work [50] can be used to explain the faster charge transfer kinetics in the MgCl<sub>2</sub>-S2 electrolyte. In the first step, the divalent Mg<sup>2+</sup> ion cluster gains one electron and undergoes the solvation sheath reorganization to become a solvated monovalent Mg<sup>+</sup> ion. In the second step, the monovalent Mg<sup>+</sup> ion cluster dissociates one solvent coordination site to form the surface adsorbed ion. The reaction rates of these two steps are determined by the Marcus electron transfer activation free energy ( $\Delta G_1^\ddagger$ ) and the desolvation activation free energy ( $\Delta G_2^\ddagger$ ), respectively, and apparent activation free energy ( $\Delta G^\ddagger$ ) is determined by the larger one between  $\Delta G_1^\ddagger$  and  $\Delta G_2^\ddagger$ . Since the structures of solvated Mg<sup>2+</sup> ions has been resolved by MLMD in the previous chapter, we calculate the  $\Delta G_1^\ddagger$  and  $\Delta G_2^\ddagger$  of solvated Mg<sup>2+</sup> ions predominantly exist (Figure S11) in the MgCl<sub>2</sub>-S2 electrolyte and the Mg(TFSI)<sub>2</sub>-S2 electrolyte (Table S1). To exhibit the influence of the coordination of Cl<sup>-</sup> ions on  $\Delta G^\ddagger$ , the Gibbs free energy curves of the solvation structure of classical trimolecular coordination, namely, Mg(S2)<sub>3</sub>, after substitution by one or two Cl<sup>-</sup> ions is shown in the Fig. 5a. According to the study in our previous work, as for the S2 solvent, the  $\Delta G_1^\ddagger$  is lower than the  $\Delta G_2^\ddagger$  during the Mg deposition process, indicating the rate-determining step in the Mg(TFSI)<sub>2</sub>-S2 electrolyte system is the desolvation process. After the Cl<sup>-</sup> ions enter into the first solvated layer of Mg<sup>2+</sup> ions, the energy

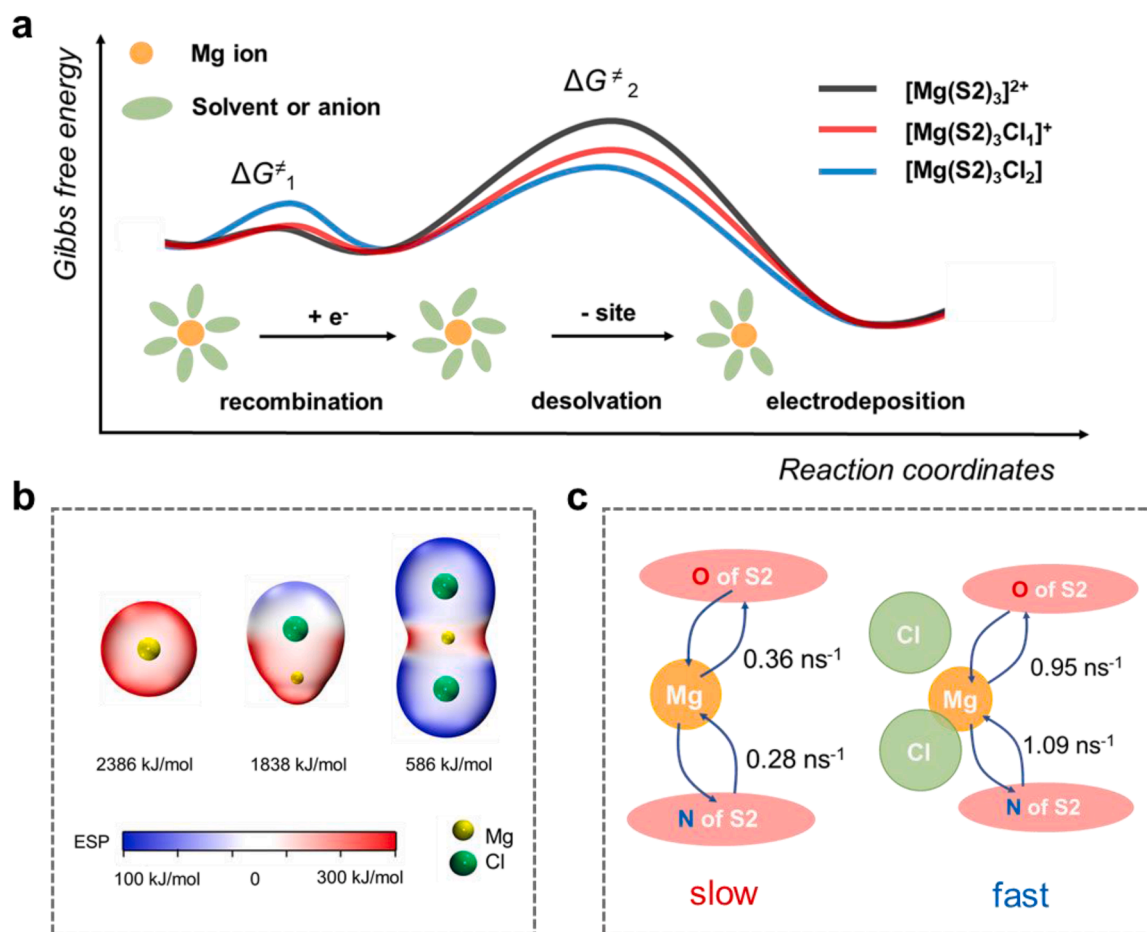


Fig. 5. a) Gibbs activation free energy in the interface electrochemical reaction processes for  $[\text{Mg}(\text{S}2)_3]^{2+}$ ,  $[\text{Mg}(\text{S}2)_3\text{Cl}]^+$  and  $[\text{Mg}(\text{S}2)_3\text{Cl}_2]$ . b) The distribution of ESP in  $\text{Mg}^{2+}$ ,  $\text{MgCl}^+$  and  $\text{MgCl}_2$  species. The maxima of ESP values are marked. c) The ligand exchange rates of  $\text{MgCl}_2$ -S2 electrolyte and  $\text{Mg}(\text{TFSI})_2$ -S2 electrolyte at 400 K obtained in the MLMD simulated trajectories.

barriers of the first step ( $\Delta G_1^\ddagger$ ) increase while the energy barriers of the second step ( $\Delta G_2^\ddagger$ ) decrease. And the  $\Delta G^\ddagger$  shows the same tendency with  $\Delta G_2^\ddagger$  due to the rate-determining step is still the desolvation process even the solvated  $\text{Mg}^{2+}$  ion cluster has coordinated with two  $\text{Cl}^-$  ions. To further investigate the reason for the change of  $\Delta G_1^\ddagger$  and  $\Delta G_2^\ddagger$ , we analyze the ESP of the  $\text{Mg}^{2+}$  ions after coordinating with different numbers of  $\text{Cl}^-$  ions. Fig. 5b shows that the positively charged region around the  $\text{Mg}^{2+}$  ion is obviously continuous contraction and value of the maximum ESP decreases gradually as well after the  $\text{Mg}^{2+}$  ion combines with one and two  $\text{Cl}^-$  ions in sequence. According to the electron density difference diagram (Figure S12a-d), after the  $\text{Cl}^-$  ions coordinate with the  $\text{Mg}^{2+}$  ion, some electrons are transferred from the  $\text{Cl}^-$  ion to the  $\text{Mg}^{2+}$  ion, demonstrating that the decrease in the positive charge of the  $\text{Mg}^{2+}$  ion is not only just caused by the simple superposition of the negative charge of the  $\text{Cl}^-$  ion, but also attributed to the chemical effect due to the electrons transfer. The coordination of  $\text{Cl}^-$  ions significantly reduces the equivalent charge of the  $\text{Mg}^{2+}$  ions and weakens the coordination ability of the  $\text{Mg}^{2+}$  ions to the S2 solvent, thus leading to the increase of solvation sheath reorganization energy and a decrease of desolvation energy. The ligand exchange rates obtained in the MLMD simulated trajectories also confirm the trend of faster desolvation process in the  $\text{MgCl}_2$ -S2 electrolyte (Fig. 5c). In the  $\text{Mg}(\text{TFSI})_2$ -S2 electrolyte, the exchange rate of O atoms in the S2 molecules with  $\text{Mg}^{2+}$  ions is  $0.36 \text{ ns}^{-1}$ , and that of N atoms is  $0.28 \text{ ns}^{-1}$ . In sharp contrast, as for the  $\text{MgCl}_2$ -S2 electrolyte, due to the reduction of the equivalent charge of the  $\text{Mg}^{2+}$  ions after combining with  $\text{Cl}^-$  ions, the exchange rates of O atoms and N atoms in the S2 molecules are increased to  $0.95$  and  $1.09 \text{ ns}^{-1}$ , respectively, a nearly three-fold rate enhancement. Although the trajectories reflect the solvent exchange rates of  $\text{Mg}^{2+}$  ions rather than  $\text{Mg}^+$  ions, the above analysis can also demonstrate the trend that the introduction of  $\text{Cl}^-$  ions accelerates the ligand exchange, leading to a fast desolvation process. This discovery can provide a brand idea to design an appropriate solvation structure via regulating anion to achieve rapid deposition kinetics and can also serve as an important clue to comprehensively understand the great improvement of  $\text{MgCl}_2$  additive to reduce the overpotential and enhance the cycling stability in other electrolyte systems. Additionally, the ligand exchange rates of  $\text{Mg}^{2+}$  ions reach the nanosecond level, which is far from being covered by AIMD. Therefore, simulations using MLMD for tens of nanoseconds are necessary to adequately explore the phase space and obtain precise dynamic solvation structures of Mg electrolytes.

### 3. Conclusion

In summary, a low-cost  $\text{MgCl}_2$ -S2 electrolyte which possesses the advantages of high interface stability and fast charge transfer kinetics for RMBs has been developed. The interface stability and charge transfer kinetics are investigated by MLMD combined with the experimental results. The amine solvent S2 greatly increases the solubility of  $\text{MgCl}_2$  due to the stronger interactions of the amino group with  $\text{Mg}^{2+}$  and  $\text{Cl}^-$  ions, allowing the cheap  $\text{MgCl}_2$  salt to be used as a single solute to support the cycling of the Mg batteries. The accurate solvation structures, along with their proportions and the rate of mutual transformation are obtained by MLMD. Furthermore, based on these accurate dynamic structures, the electronic structure which can determine the electrochemical behaviors of the electrolytes is analyzed. The results show that the degree of dissociation in  $\text{MgCl}_2$ -S2 electrolyte is less than 1 %, much lower than 95.1 % in  $\text{MgTFSI}_2$ -S2 electrolyte. The easier entry of the  $\text{Cl}^-$  anions into the  $\text{Mg}^{2+}$  solvation layers changes the energy band structure of the electrolyte so that  $\text{Mg}^{2+}$  ions can gain electrons in preference to anions in thermodynamics and thus improve the stability of the interface. Moreover,  $\text{Cl}^-$  ions in solvated sheath partially shell the high charge density of  $\text{Mg}^{2+}$  ions, thereby improving the desolvation rates by nearly 3 times, and further enhancing the deposition kinetics. Therefore, the  $\text{MgCl}_2$ -S2 electrolyte exhibits an ultra-long cycle life in Mg//SS asymmetric cell for over 4500 cycles (about 12 months) with an

outstanding CE about 99.2 %, which is much better than those of the reference  $\text{Mg}(\text{TFSI})_2$ -S2 electrolyte. This work inspires a new paradigm from machine learning molecular dynamics to study interface reaction and develop the high-effectively electrolytes.

### Experimental section

Experimental details are provided in Supporting Information.

Data Availability

The data are available on request from the corresponding author.

### CRediT authorship contribution statement

**Haiming Hua:** Writing – original draft, Software, Methodology, Investigation, Formal analysis, Data curation, Conceptualization. **Fei Wang:** Writing – original draft, Methodology, Investigation, Formal analysis, Data curation, Conceptualization. **Feng Wang:** Writing – review & editing, Software, Data curation. **Jiayue Wu:** Writing – review & editing, Data curation. **Yaoqi Xu:** Methodology. **Yichao Zhuang:** Writing – review & editing. **Jing Zeng:** Writing – review & editing, Supervision, Project administration, Funding acquisition, Conceptualization. **Jinbao Zhao:** Writing – review & editing, Supervision, Resources, Project administration, Funding acquisition.

### Declaration of competing interest

The authors declare that they have no known competing financial interests or personal relationships that could have appeared to influence the work reported in this paper.

### Acknowledgments

The authors gratefully acknowledge the National Key Research and Development Program of China (No. 2021YFB2400300), Natural Science Foundation of China (Nos. 21875198, 22005257, and 22021001), Natural Science Foundation of Fujian Province of China (No.2020J05009) for financial support. Numerical computations were performed on Hefei advanced computing center.

### Supplementary materials

Supplementary material associated with this article can be found, in the online version, at [doi:10.1016/j.ensm.2024.103470](https://doi.org/10.1016/j.ensm.2024.103470).

### References

- [1] J.B. Goodenough, K.-S. Park, The Li-ion rechargeable battery: a perspective, *J. Am. Chem. Soc.* 135 (4) (2013) 1167–1176, <https://doi.org/10.1021/ja3091438>.
- [2] R.M. Vinodkumar Etacheri, Ran Elazari, Gregory Salitra, Doron Aurbach, Challenges in the development of advanced Li-ion batteries—a review, *Energy Environ. Sci.* 4 (9) (2011) 3243–3262, <https://doi.org/10.1039/c1ee01598b>.
- [3] X. Zhang, Y.A. Yang, Z. Zhou, Towards practical lithium-metal anodes, *Chem. Soc. Rev.* 49 (10) (2020) 3040–3071, <https://doi.org/10.1039/c9cs00838a>.
- [4] J. Zhang, Z. Chang, Z. Zhang, A. Du, S. Dong, Z. Li, G. Li, G. Cui, Current design strategies for rechargeable magnesium-based batteries, *ACS Nano* 15 (10) (2021) 15594–15624, <https://doi.org/10.1021/acsnano.1c06530>.
- [5] R. Mohtadi, O. Tutusaus, T.S. Arthur, Z. Zhao-Karger, M. Fichtner, The metamorphosis of rechargeable magnesium batteries, *Joule* 5 (3) (2021) 581–617, <https://doi.org/10.1016/j.joule.2020.12.021>.
- [6] F.F. Liu, T.T. Wang, X.B. Liu, L.Z. Fan, Challenges and recent progress on key materials for rechargeable magnesium batteries, *Adv. Energy Mater.* 11 (2) (2021) 28, <https://doi.org/10.1002/aenm.202000787>.
- [7] Z. Liang, C. Ban, Strategies to enable reversible magnesium electrochemistry: from electrolytes to artificial solid-electrolyte interphases, *Angew. Chem. Int. Edit.* 60 (20) (2021) 11036–11047, <https://doi.org/10.1002/anie.202006472>.
- [8] D. Wu, F. Wang, H. Yang, Y. Xu, Y. Zhuang, J. Zeng, Y. Yang, J. Zhao, Realizing rapid electrochemical kinetics of  $\text{Mg}^{2+}$  in Ti-Nb oxides through a  $\text{Li}^+$  intercalation activated strategy toward extremely fast charge/discharge dual-ion batteries, *Energy Storage Mater.* 52 (2022) 94–103, <https://doi.org/10.1016/j.ensm.2022.07.042>.
- [9] J. Zeng, D.Z. Wu, X. Wang, J.N. Wu, J.Y. Li, J. Wang, J.B. Zhao, Insights into the Mg storage property and mechanism based on the honeycomb-like structured

- Na3V2(P04)(3)/C/G in anhydrous electrolyte, *Chem. Eng. J.* 372 (2019) 37–45, <https://doi.org/10.1016/j.ccej.2019.04.128>.
- [10] X.J. Zhou, G.Y. Li, Y.F. Yu, M. Lei, K.Y. Chen, C.L. Li, Building organic-inorganic robust interphases from deep eutectic solution for highly stable mg metal anode in conventional electrolyte, *Small Methods* 11 (2023), <https://doi.org/10.1002/smt.202301109>.
- [11] M. Hu, G.Y. Li, K.Y. Chen, X.J. Zhou, C.L. Li, A gradient structured SEI enabling record-high areal capacity anode for high-rate Mg metal batteries, *Chem. Eng. J.* 480 (2024) 10, <https://doi.org/10.1016/j.ccej.2023.148193>.
- [12] Y.J. Li, X.J. Zhou, J.L. Hu, Y.J. Zheng, M.S. Huang, K. Guo, C.L. Li, Reversible Mg metal anode in conventional electrolyte enabled by durable heterogeneous SEI with low surface diffusion barrier, *Energy Storage Mater.* 46 (2022) 1–9, <https://doi.org/10.1016/j.ensm.2021.12.023>.
- [13] Z. Guo, S. Zhao, T. Li, D. Su, S. Guo, G. Wang, Recent advances in rechargeable magnesium-based batteries for high-efficiency energy storage, *Adv. Energy Mater.* 10 (21) (2020) 17, <https://doi.org/10.1002/aenm.201903591>.
- [14] P. Bonnicks, J. Muldoon, A trip to Oz and a peak behind the curtain of magnesium batteries, *Adv. Funct. Mater.* 30 (21) (2020) 15, <https://doi.org/10.1002/adfm.201910510>.
- [15] Z. Ma, D.R. MacFarlane, M. Ka, Mg cathode materials and electrolytes for rechargeable Mg batteries: a review, *Batteries Supercaps* 2 (2) (2019) 115–127, <https://doi.org/10.1002/batt.201800102>.
- [16] J. Muldoon, C.B. Bucur, T. Gregory, Fervent hype behind magnesium batteries: an open call to synthetic chemists—electrolytes and cathodes needed, *Angew. Chem. Int. Edit.* 56 (40) (2017) 12064–12084, <https://doi.org/10.1002/anie.201700673>.
- [17] P. Saha, M.K. Datta, O.I. Velikokhatnyi, A. Manivannan, D. Alman, P.N. Kumta, Rechargeable magnesium battery: current status and key challenges for the future, *Prog. Mater. Sci.* 66 (2014) 1–86, <https://doi.org/10.1016/j.pmatsci.2014.04.001>.
- [18] C.L. You, X.W. Wu, X.H. Yuan, Y.H. Chen, L.L. Liu, Y.S. Zhu, L.J. Fu, Y.P. Wu, Y. G. Guo, T. van Ree, Advances in rechargeable Mg batteries, *J. Mater. Chem. A* 8 (48) (2020) 25601–25625, <https://doi.org/10.1039/d0ta09330k>.
- [19] O. Mizrahi, N. Amir, E. Pollak, O. Chusid, V. Marks, H. Gottlieb, L. Larush, E. Zinigrad, D. Aurbach, Electrolyte solutions with a wide electrochemical window for recharge magnesium batteries, *J. Electrochem. Soc.* 155 (2) (2008) A103–A109, <https://doi.org/10.1149/1.2806175>.
- [20] D. Aurbach, Z. Lu, A. Schechter, Y. Gofer, H. Gizbar, R. Turgeman, Y. Cohen, M. Moshkovich, E. Levi, Prototype systems for rechargeable magnesium batteries, *Nature* 407 (6805) (2000) 724–727, <https://doi.org/10.1038/35037553>.
- [21] N. Pour, Y. Gofer, D.T. Major, D. Aurbach, Structural analysis of electrolyte solutions for rechargeable mg batteries by stereoscopic means and DFT Calculations, *J. Am. Chem. Soc.* 133 (16) (2011) 6270–6278, <https://doi.org/10.1021/ja1098512>.
- [22] T.J. Carter, R. Mohtadi, T.S. Arthur, F. Mizuno, R. Zhang, S. Shirai, J.W. Kampf, Boron clusters as highly stable magnesium-battery electrolytes, *Angew. Chem. Int. Edit.* 53 (12) (2014) 3173–3177, <https://doi.org/10.1002/anie.201310317>.
- [23] A.B. Du, Z.H. Zhang, H.T. Qu, Z.L. Cui, L.X. Qiao, L.L. Wang, J.C. Chai, T. Lu, S. M. Dong, T.T. Dong, H.M. Xu, X.H. Zhou, G.L. Cui, An efficient organic magnesium borate-based electrolyte with non-nucleophilic characteristics for magnesium-sulfur battery, *Energy Environ. Sci.* 10 (12) (2017) 2616–2625, <https://doi.org/10.1039/c7ee02304a>.
- [24] R. Attias, M.S. Chae, B. Dlugatch, M. Olie, Y. Goffer, D. Aurbach, The Role of Surface Adsorbed Cl- Complexes in Rechargeable Magnesium Batteries, *ACS Catal.* 10 (14) (2020) 7773–7784, <https://doi.org/10.1021/acscatal.0c01956>.
- [25] R. Mohtadi, M. Matsui, T.S. Arthur, S.J. Hwang, Magnesium borohydride: from hydrogen storage to magnesium battery, *Angew. Chem. Int. Edit.* 51 (39) (2012) 9780–9783, <https://doi.org/10.1002/anie.201204913>.
- [26] O. Tutusaus, R. Mohtadi, T.S. Arthur, F. Mizuno, E.G. Nelson, Y.V. Sevryugina, An efficient halogen-free electrolyte for use in rechargeable magnesium batteries, *Angew. Chem. Int. Edit.* 54 (27) (2015) 7900–7904, <https://doi.org/10.1002/anie.201412202>.
- [27] T.D. Gregory, R.J. Hoffman, R.C. Winterton, Nonaqueous electrochemistry of magnesium: applications to energy storage, *J. Electrochem. Soc.* 137 (3) (1990) 775–780, <https://doi.org/10.1149/1.2086553>.
- [28] Z. Lu, A. Schechter, M. Moshkovich, D. Aurbach, On the electrochemical behavior of magnesium electrodes in polar aprotic electrolyte solutions, *J. Electroanal. Chem.* 466 (2) (1999) 203–217, [https://doi.org/10.1016/s0022-0728\(99\)00146-1](https://doi.org/10.1016/s0022-0728(99)00146-1).
- [29] D. Aurbach, H. Gizbar, A. Schechter, O. Chusid, H.E. Gottlieb, Y. Gofer, I. Goldberg, Electrolyte solutions for rechargeable magnesium batteries based on organomagnesium chloroaluminate complexes, *J. Electrochem. Soc.* 149 (2) (2002) A115–A121, <https://doi.org/10.1149/1.1429925>.
- [30] R.E. Doe, R. Han, J. Hwang, A.J. Gmitter, I. Shterenberg, H.D. Yoo, N. Pour, D. Aurbach, Novel, electrolyte solutions comprising fully inorganic salts with high anodic stability for rechargeable magnesium batteries, *Chem. Commun.* 50 (2) (2014) 243–245, <https://doi.org/10.1039/c3cc47896c>.
- [31] S.B. Son, T. Gao, S.P. Harvey, K.X. Steirer, A. Stokes, A. Norman, C.S. Wang, A. Cresce, K. Xu, C.M. Ban, An artificial interphase enables reversible magnesium chemistry in carbonate electrolytes, *Nat. Chem.* 10 (5) (2018) 532–539, <https://doi.org/10.1038/s41557-018-0019-6>.
- [32] J.H. Xiao, X.X. Zhang, H.Y. Fan, Y.X. Zhao, Y. Su, H.W. Liu, X.Z. Li, Y.P. Su, H. Yuan, T. Pan, Q.Y. Lin, L.D. Pan, Y.G. Zhang, Stable solid electrolyte interphase in situ formed on magnesium-metal anode by using a perfluorinated alkoxide-based all-magnesium salt electrolyte, *Adv. Mater.* 34 (30) (2022) 9, <https://doi.org/10.1002/adma.202203783>.
- [33] Y.M. Zhao, A.B. Du, S.M. Dong, F. Jiang, Z.Y. Guo, X.S. Ge, X.L. Qu, X.H. Zhou, G. L. Cui, A bismuth-based protective layer for magnesium metal anode in noncorrosive electrolytes, *ACS Energy Lett.* 6 (7) (2021) 2594–2601, <https://doi.org/10.1021/acscenergylett.1c01243>.
- [34] R.J. Lv, X.Z. Guan, J.H. Zhang, Y.Y. Xia, J.Y. Luo, Enabling Mg metal anodes rechargeable in conventional electrolytes by fast ionic transport interphase, *Natl. Sci. Rev.* 7 (2) (2020) 333–341, <https://doi.org/10.1093/nsr/nwz1157>.
- [35] C. Pechberly, A. Bagopian, J.B. Ledeuil, D. Foix, J. Allouche, J.N. Chotard, O. Luzanin, J. Bitenc, R. Dominko, R. Dedryvere, J.S. Filhol, L. Stievano, R. Berthelot, Alloying electrode coatings towards better magnesium batteries, *J. Mater. Chem. A* 10 (22) (2022) 12104–12113, <https://doi.org/10.1039/d2ta02083a>.
- [36] Y.Y. Hwang, N.K. Lee, S.H. Park, J. Shin, Y.J. Lee, TFSS anion grafted polymer as an ion-conducting protective layer on magnesium metal for rechargeable magnesium batteries, *Energy Storage Mater.* 51 (2022) 108–121, <https://doi.org/10.1016/j.ensm.2022.06.014>.
- [37] C.Y. Wang, Y. Huang, Y.H. Lu, H.G. Pan, B.B. Xu, W.P. Sun, M. Yan, Y.Z. Jiang, Reversible magnesium metal anode enabled by cooperative solvation/surface engineering in carbonate electrolytes, *Nano-Micro Lett* 13 (1) (2021) 11, <https://doi.org/10.1007/s40820-021-00716-1>.
- [38] E. Sahadeo, G. Rubloff, S.B. Lee, C.F. Lin, Al2O3 thin films on magnesium: assessing the impact of an artificial solid electrolyte interphase, *Front. Energy Res.* 9 (2021) 11, <https://doi.org/10.3389/fenrg.2021.618368>.
- [39] Y. Li, P. Zuo, R. Li, H. Huo, Y. Ma, C. Du, Y. Gao, G. Yin, R.S. Weatherup, Formation of an artificial Mg2+-permeable interphase on Mg anodes compatible with ether and carbonate electrolytes, *ACS Appl. Mater. Interfaces* 13 (2021) 24565–24574, <https://doi.org/10.1021/acami.0c22520>.
- [40] K. Tang, A.B. Du, X.F. Du, S.M. Dong, C.L. Lu, Z.L. Cui, L.S. Li, G.L. Ding, F.X. Chen, X.H. Zhou, G.L. Cui, A novel regulation strategy of solid electrolyte interphase based on anion-solvent coordination for magnesium metal anode, *Small* 16 (49) (2020) 8, <https://doi.org/10.1002/sml.202005424>.
- [41] K. Tang, A.B. Du, S.M. Dong, Z.L. Cui, X. Liu, C.L. Lu, J.W. Zhao, X.H. Zhou, G. L. Cui, A stable solid electrolyte interphase for magnesium metal anode evolved from a bulky anion lithium salt, *Adv. Mater.* 32 (6) (2020) 7, <https://doi.org/10.1002/adma.201904987>.
- [42] B. Li, R. Masse, C.F. Liu, Y. Hu, W.S. Li, G.Q. Zhang, G.Z. Cao, Kinetic surface control for improved magnesium-electrolyte interfaces for magnesium ion batteries, *Energy Storage Mater.* 22 (2019) 96–104, <https://doi.org/10.1016/j.ensm.2019.06.035>.
- [43] W.Y. Zhao, Z.H. Pan, Y.J. Zhang, Y. Liu, H.L. Dou, Y.Y. Shi, Z.J. Zuo, B.W. Zhang, J. P. Chen, X.L. Zhao, X.W. Yang, Tailoring coordination in conventional ether-based electrolytes for reversible magnesium-metal anodes, *Angew. Chem. Int. Edit.* 61 (30) (2022) 9, <https://doi.org/10.1002/anie.202205187>.
- [44] Y.Y. Du, Y.M. Chen, S.S. Tan, J.L. Chen, X.T. Huang, L.M. Cui, J.C. Long, Z. T. Wang, X.H. Yao, B. Shang, G.S. Huang, X.Y. Zhou, L.J. Li, J.F. Wang, F.S. Pan, Strong solvent coordination effect inducing gradient solid-electrolyte-interphase formation for highly efficient Mg plating/stripping, *Energy Storage Mater.* 62 (2023) 12, <https://doi.org/10.1016/j.ensm.2023.102939>.
- [45] D. Zhang, Y.R. Wang, Y. Yang, Y. Zhang, Y.Z. Zhao, M. Pan, Y.K. Sun, S.P. Chen, X. S. Liu, J.L. Wang, Y. NuLi, Constructing Efficient Mg(CF3SO3)2 electrolyte via tailoring solvation and interface chemistry for high-performance rechargeable magnesium batteries, *Adv. Energy Mater.* (2023) 13, <https://doi.org/10.1002/aenm.202301795>.
- [46] S.Y. Wang, K.W. Wang, Y.C. Zhang, Y.L. Jie, X.P. Li, Y.X. Pan, X.W. Gao, Q.S. Nian, R.G. Cao, Q. Li, S.H. Jiao, D.S. Xu, High-entropy electrolyte enables high reversibility and long lifespan for magnesium metal anodes, *Angew. Chem. Int. Edit.* 10 (2023), <https://doi.org/10.1002/anie.202304411>.
- [47] Y. Liu, W.Y. Zhao, Z.H. Pan, Z.Q. Fan, M. Zhang, X.L. Zhao, J.P. Chen, X.W. Yang, Interfacial engineering of magnesiophilic coordination layer stabilizes Mg metal anode, *Angew. Chem. Int. Edit.* 62 (25) (2023) 6, <https://doi.org/10.1002/anie.202302617>.
- [48] J.L. Zhang, J. Liu, M. Wang, Z.H. Zhang, Z.F. Zhou, X. Chen, A.B. Du, S.M. Dong, Z. J. Li, G.C. Li, G.L. Cui, The origin of anode-electrolyte interfacial passivation in rechargeable Mg-metal batteries, *Energy Environ. Sci.* 16 (3) (2023) 1111–1124, <https://doi.org/10.1039/d2ee03270h>.
- [49] S. Hou, X. Ji, K. Gaskell, P.-F. Wang, L. Wang, J. Xu, R. Sun, O. Borodin, C. Wang, Solvation sheath reorganization enables divalent metal batteries with fast interfacial charge transfer kinetics, *Science* (1979) 374 (6564) (2021) 172–178, <https://doi.org/10.1126/science.abg3954>.
- [50] F. Wang, H. Hua, D. Wu, J. Li, Y. Xu, X. Nie, Y. Zhuang, J. Zeng, J. Zhao, Solvent molecule design enables excellent charge transfer kinetics for a magnesium metal anode, *ACS Energy Lett.* 8 (1) (2023) 780–789, <https://doi.org/10.1021/acscenergylett.2c02525>.
- [51] F. Wang, Y. Sun, J. Cheng, Switching of redox levels leads to high reductive stability in water-in-salt electrolytes, *J. Am. Chem. Soc.* 9 (2023), <https://doi.org/10.1021/jacs.2c11793>.
- [52] F. Wang, J. Cheng, Automated workflow for computation of redox potentials, acidity constants, and solvation free energies accelerated by machine learning, *J. Chem. Phys.* 157 (2) (2022) 8, <https://doi.org/10.1063/5.0098330>.
- [53] F. Wang, J. Cheng, Understanding the solvation structures of glyme-based electrolytes by machine learning molecular dynamics, *Chin. J. Struct. Chem.* 42 (9) (2023) 7, <https://doi.org/10.1016/j.cjcs.2023.100061>.
- [54] J.C. Liu, R.X. Liu, Y. Cao, M.H. Chen, Solvation structures of calcium and magnesium ions in water with the presence of hydroxide: a study by deep potential molecular dynamics, *Phys. Chem. Chem. Phys.* 25 (2) (2023) 983–993, <https://doi.org/10.1039/d2cp04105g>.

- [55] L.F. Zhang, J.Q. Han, H. Wang, R. Car, E. Weinan, Deep potential molecular dynamics: a scalable model with the accuracy of quantum mechanics, *Phys. Rev. Lett.* 120 (14) (2018) 6, <https://doi.org/10.1103/PhysRevLett.120.143001>.
- [56] Y. Zhang, H. Wang, W. Chen, J. Zeng, L. Zhang, H. Wang, E. W, DP-GEN: a concurrent learning platform for the generation of reliable deep learning based potential energy models, *Comput. Phys. Commun.* 253 (2020) 107206, <https://doi.org/10.1016/j.cpc.2020.107206>.
- [57] H. Wang, L. Zhang, J. Han, E. W, DeepMD-kit: a deep learning package for many-body potential energy representation and molecular dynamics, *Comput. Phys. Commun.* 228 (2018) 178–184, <https://doi.org/10.1016/j.cpc.2018.03.016>.
- [58] S. Eisler, R. McDonald, G.R. Loppnow, R.R. Tykwinski, Structural, vibrational, and electronic characteristics of enyne macrocycles as a function of ring strain, *J. Am. Chem. Soc.* 122 (29) (2000) 6917–6928, <https://doi.org/10.1021/ja000617g>.
- [59] J.A. Guerrero-Alvarez, A. Ariza-Castolo, Correlation between  $^{13}\text{C}$  and  $^{17}\text{O}$  chemical shifts and torsional strain in spiroacetals, *Tetrahedron. Lett.* 48 (5) (2007) 795–798, <https://doi.org/10.1016/j.tetlet.2006.11.162>.
- [60] S.S. Lin, H.M. Hua, P.B. Lai, J.B. Zhao, A Multifunctional dual-salt localized high-concentration electrolyte for fast dynamic high-voltage lithium battery in wide temperature range, *Adv. Energy Mater.* 11 (36) (2021) 10, <https://doi.org/10.1002/aenm.202101775>.
- [61] K. Sodeyama, Y. Yamada, K. Aikawa, A. Yamada, Y. Tateyama, Sacrificial anion reduction mechanism for electrochemical stability improvement in highly concentrated Li-Salt electrolyte, *J. Phys. Chem. C* 118 (26) (2014) 14091–14097, <https://doi.org/10.1021/jp501178n>.
- [62] A. Morag, X.Y. Chu, C. Neumann, D. Pohl, M. Borrelli, D. Sabaghi, M. Löffler, Z. Sofer, A. Turchanin, M.H. Yu, X.L. Feng, Ionic liquid electrolyte additive regulates the multi-species-insertion titanium sulfide cathode for magnesium batteries, *Energy Storage Mater.* 53 (2022) 435–443, <https://doi.org/10.1016/j.ensm.2022.09.021>.